تحليل عددي للتشوه الناتج عن الرطوبة في السدود الحجرية

تشيوائمينغلي * ، أونلونغليو**

* تشيوائمينغلي، الأكاديمية الصينية لعلوم وتكنولوجيا السلامة، بكين 100012، الصين .

البريدالإلكتروني: 454968503@qq.com، التخصص: الهندسة الجيوتقنية .

** أونلونغليو، المختبرالرئيسي في الدولة لهندسة السوائل المتحركة و الأنهار الطبيعية،

كلية الموارد المائية والطاقة الكهرومائية، جامعة سيتشوان، تشنغدو 610065، الصين،

البريدالإلكتروني: liuenlonggeo@163.com. التخصص: الهندسة الجيوتقنية .

مراسلة المؤلف على البريد الالكتروني: liuenlonggeo@163.com

الخلاصة

من الممكن أن يؤدي التشوه الناتج عن الرطوبة إلى مخاطر هندسية خطيرة بالنسبة للسدود الحجرية. وكان قد تم اقتراح طريقة حسابية جديدة للتشوه الناتج عن الرطوبة وهي إجراء تحليل التشوه الضاغط على السدود الحجرية. وبناء على نتائج اختبارات الترطيب ثلاثية الابعاد للمواد الصخرية، فقد تمت دراسة تأثير الضغط المحيط على الضغط الحجمي الناتج عن الرطوبة عن طريق مراجعة نموذج سطح الخضوع المزدوج الحالي للمواد الصخرية. وقد تمت برمجة رمز العنصر المحدود غير الخطي لإجراء تحليل التشوه الضاغط على واحد من السدود الحجرية ذات الواجهة الخرسانية في ظل ظروف التسرب المستقر وارتفاع منسوب المياه الأرضية مع نموذج البلاستيك التأسيسي. وتبرهن النتائج الحسابية أن: 1 التشوه الناتج عن الرطوبة للمواد الصخرية تحت سطح التشبع له تأثير كبير على توزيع التشوه والضغط في هيكل السد. 2 مصحوبا بالتشوه الناتج عن الرطوبة، فإن تسوية جسم السد تزيد وتتحرك الإزاحة الأفقية نحو أسفل المجرى. وتظهر الزيادة الأعلى نسبيا لإجهاد الضغط في واجهة المسطح، وتزداد ذروة القيم في كل من الجهد الضاغط والمكثف في الاتجاه الأفقي.

Numerical analysis of wetting-induced deformation of rockfill dams

Quan-Ming Li* and En-Long Liu**

*** China Academy of Safety Science and Technology, Beijing 100012, China; Email: 454968503@qq.com;
Specialty: Geotechnical Engineering;*

*** State Key Laboratory of Hydraulics and Natural River Engineering, College of Water Resource and
Hydropower, Sichuan University, Chengdu 610065, China; Email: liuenlonggeo@163.com; Specialty:
Geotechnical Engineering.*

**Corresponding Author: En-Long Liu. Tel: +86 28 85405121. Email: liuenlonggeo@163.com.*

ABSTRACT

Wetting-induced deformation can lead to serious engineering hazards in rockfill dams. A new computational method for the determination of wetting-induced deformation is proposed here, which performs stress-deformation analysis of rockfill dams. Based on the results of triaxial wetting tests of rockfill materials, the effect of confining pressure on the wetting-induced volumetric strain was considered by revising the existing double-yielding surface model for rockfill materials. The nonlinear finite element code was programed to perform stress-deformation analysis on a concrete-faced rockfill dam under the conditions of steady seepage and rise in tail water table using an elastoplastic constitutive model. The computational results demonstrate that (i) the wetting-induced deformation of rockfill materials under the phreatic line has significant effects on the distribution of deformation and stress in the dam body; (ii) along with the wetting-induced deformation, there is an increase in the settlement of the dam body and the horizontal displacement moves downstream. A relatively higher increment of compressive stress appears in the face slab and the peak values of both compressive and extensive stresses in the horizontal direction increase.

Keywords: Wetting-induced deformation; numerical analysis; rockfill dam; finite element method.

INTRODUCTION

Wetting-induced deformation of rockfill materials occurs when these materials are saturated from their initial dry or unsaturated state. When the rockfill materials are immersed in water, the minerals in the soil particles may start softening, which leads to the sliding, breaking, and rearrangement of soil particles. Thus, wetting-induced deformation occurs (Saboya and Byrne, 1993). Upon the initial impounding, many soil dams with core walls develop engineering problems including longitudinal cracks near the dam crests, transverse cracks at the dam ends, and displacements of core-walls and dam crests in the upstream direction because of the wetting-induced deformation of dam materials located upstream. Many engineering incidents have occurred because of the wetting-induced deformation of dams. Therefore, it is important to predict and compute the wetting-induced deformation of rockfill dams.

Several studies, including laboratory tests and theoretical and numerical analyses, have been

performed to study the wetting-induced deformation (Alonso et al., 1990; Ferber et al., 2008). It has been indicated that there are many factors that affect the wetting-induced deformation. Some of the main factors are the mineral components in the rockfill materials, density, stress level and state, stress path, water content, duration of wetting, and the sample size and simulation methods utilized for the rockfill dam. Initially, a plane strain finite element program was employed to compute the wetting-induced deformation of dams during reservoir filling using the Duncan-Chang nonlinear elastic constitutive model (Duncan and Chang, 1970) of rockfill materials, which took into consideration the effects of seepage and buoyant loads on soil masses (Nobari and Duncan, 1972). After analyzing the nonlinear elastic procedure widely used in the wetting-induced deformation in rockfill dams, Escuder et al. (2005) proposed a new wetting simulation procedure and employed it to compute the constructional behavior and wetting effects of a 100 m high structure, and the calculation routines have been incorporated into the fast Lagrangian analysis of continua. The computed results demonstrated that it is useful in predicting wetting-induced settlements in the upstream shells of earth-core dams. Cen et al. (2009) used the Gudehus-Bauer hypoplastic model to analyze the deformation in rockfill dams due to the change in moisture content, and numerical simulation was used to simulate the evolution of deformation and stress in a core-wall type rockfill dam during the first water impounding. Roosta and Alizadeh (2012) used a nonlinear strain hardening-strain softening model to simulate the behavior of rockfill materials and introduced a collapse coefficient to display wetting-induced settlement. Large-scale triaxial tests of rockfill materials were simulated, and it was demonstrated that the method could be used with any suitable constitutive model of other coarse-grained materials to identify collapse settlements due to saturation. Zou et al. (2015) used the generalized plasticity model and the wetting model based on the wetting tests on a Xi, yi conglomerate gravel to perform numerical analysis of wetting-induced collapse of an asphalt concrete core dam. The results of this analysis demonstrated that the generalized plastic model combined with the wetting model could reflect the wetting deformation and stress distribution of the dam. Various elastoplastic constitutive models for rockfill materials are used to compute the wetting-induced deformation but the methods proposed in the above studies to compute wetting-induced deformation of dams are distinct and lack a unified approach. Therefore, there is a need for further study.

In this paper, a new numerical simulation of wetting-induced deformation is formulated based on the triaxial wetting tests of rockfill materials, in which the influence of confining pressure on the wetting-induced volumetric strain is taken into account, and a finite element code that considers the wetting-induced deformation is programed based on the nonlinear analysis code of TOSS3D (Zhu and Shen, 1990). Next, a numerical method is employed to simulate the wetting-induced deformation of a concrete-faced rockfill dam under the conditions of steady seepage and rise in tail water table, and the effects of wetting-induced deformation on stress and deformation of a concrete-faced dam are analyzed in detail.

CONSTITUTIVE MODEL

The constitutive model for rockfill materials

The double-yielding surface model proposed by Shen (2000) was used here to model the stress-

strain relationship of rockfill materials. As shown in Fig. 1, there are two yielding surfaces in the model, in which f_1 represents the volumetric-yielding surface and f_2 represents the shear-yielding surface. These are expressed as follows:

$$f_1 = p^2 + r^2 q^2 \tag{1}$$

and

$$f_2 = q^s / p \tag{2}$$

where $p = (\sigma_1 + \sigma_2 + \sigma_3)/3$, $q = \frac{1}{\sqrt{2}}\left[(\sigma_1 - \sigma_2)^2 + (\sigma_2 - \sigma_3)^2 + (\sigma_3 - \sigma_1)^2\right]$, and r and s are model parameters. Both r and s have the value of 2.0 for rockfill materials (Shen, 2000).
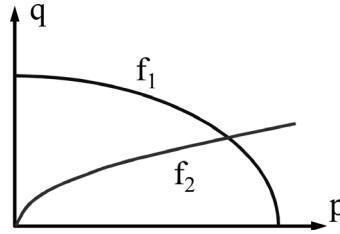
Figure 1. Yielding surfaces in the double-yielding surface model.

According to the plasticity theory of soil, the volumetric strain $\Delta\varepsilon_v$ and the shear strain $\Delta\varepsilon_s$ in the model can be formulated as follows:

$$
\left.
\begin{aligned}
\Delta\varepsilon_v &= \frac{\Delta p}{B_e} + A_1 \frac{\partial f_1}{\partial p}\Delta p + A_2 \frac{\partial f_2}{\partial p}\Delta p \\
\Delta\varepsilon_s &= \frac{\Delta p}{B_e} + A_1 \frac{\partial f_1}{\partial q}\Delta q + A_2 \frac{\partial f_2}{\partial q}\Delta q
\end{aligned}
\right\}
\tag{3}
$$

Under triaxial stress conditions, we have $\Delta p = \Delta\sigma_1 / 3$, $\Delta q = \Delta\sigma_1$, $\varepsilon_s = \Delta\varepsilon_1 - \Delta\varepsilon_v / 3$, and by defining $E_t = \frac{\Delta\sigma_1}{\Delta\varepsilon_1}$ and $\mu_t = \frac{\Delta\varepsilon_v}{\Delta\varepsilon_1}$, we can obtain A_1 and A_2 as follows:

$$
\left.
\begin{aligned}
A_1 &= \frac{1}{4p^2} \frac{\eta\left(\dfrac{9}{E_t} - \dfrac{3\mu_t}{E_t} - \dfrac{3}{G_e}\right) + 2s\left(\dfrac{3\mu_t}{E_t} - \dfrac{1}{B_e}\right)}{2(1 + 3r^2\eta)(s + r^2\eta^2)} \\
A_2 &= \frac{p^2 q^2}{q^{2s}} \frac{\eta\left(\dfrac{9}{E_t} - \dfrac{3\mu_t}{E_t} - \dfrac{3}{G_d}\right) - 2r^2\eta\left(\dfrac{3\mu_t}{E_t} - \dfrac{1}{B_e}\right)}{2(3s - \eta)(s + r^2\eta^2)}
\end{aligned}
\right\},
\tag{4}
$$

in which $G_e = \frac{E_{ur}}{2(1+\mu)}$, $B_e = \frac{E_{ur}}{3(1-2\mu)}$, and $\eta = \frac{q}{p}$.

In the model, the q-ε_1 curve in the triaxial shear test is assumed to be a hyperbolic curve and the ε_v-ε_1 curve in the test is assumed to be a parabolic curve as shown in Fig. 2. Using a derivation similar to the Duncan-Chang model, E_t and μ_t can be obtained as follows:

$$E_t = \left[1 - \frac{R_f(1 - \sin\varphi)(\sigma_1 - \sigma_3)}{2c\cos\varphi + 2\sigma_3\sin\varphi}\right]^2 Kp_a\left(\frac{\sigma_3}{p_a}\right)^n, \tag{5}$$

where c is the cohesion, ϕ is the internal frictional angle, p_a is the standard atmospheric pressure, and K, n, R_f are model parameters.

$$\mu_t = 2C_d \left(\frac{\sigma_3}{p_a}\right)^d \frac{E_i R_f}{\sigma_1 - \sigma_3} \frac{1 - R_d}{R_d} \left[1 - \frac{S}{1-S} \frac{1-R_d}{R_d} \right],$$

(6)

where $E_i = Kp_a \left(\frac{\sigma_3}{p_a}\right)^n$ and C_d, d, and R_d are model parameters.
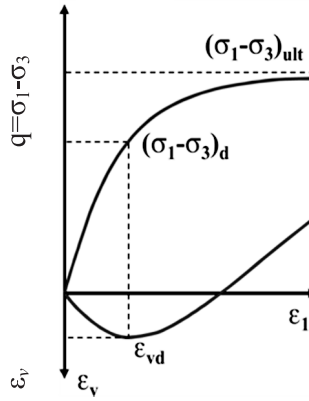
Figure 2. The q-ε_1 and ε_v-ε_1 curves assumed in the double-yielding surface model.

The revised model for computing wetting-induced deformation

In the C_w-D_w wetting model, the wetting-induced deformation can be split into wetting-induced volumetric strain ε_{vw} and wetting-induced shear strain ε_{sw}. Based on the test results of rockfill materials under wetting conditions, the following expressions for computing wetting-deformation are used.

$$\varepsilon_{vw} = \sigma_3 / \left(a + b\sigma_3 \right)$$

(7)

and

$$\varepsilon_{sw} = D_w S_l / \left(1 - S_l \right),$$

(8)

in which S_l is the stress level and $S_l = \dfrac{\left(\sigma_1 - \sigma_3\right)\left(1 - \sin\varphi\right)}{2c \cdot \cos\varphi + 2\sigma_3 \cdot \sin\varphi}$; a, b, and D_w are constants.

The principal axes of strain and stress are assumed to be the same, and the Prandtl-Reuss flow rule is used here. Therefore, the strain matrix can be obtained as follows:

$$\left[\varepsilon \right] = \frac{\varepsilon_{vw}}{3} I + \frac{\varepsilon_{sw}}{q} \left[s \right],$$

(9)

in which [s] is a deviatoric stress matrix and I is a unit matrix.

Therefore, the matrix form of the extended elastoplastic constitutive model formulated above can be given as follows:

$$\begin{bmatrix} \Delta\varepsilon_{v+vw} \\ \Delta\varepsilon_{s+sw} \end{bmatrix} = \begin{bmatrix} d_{11} & d_{12} \\ d_{21} & d_{22} \end{bmatrix} \begin{bmatrix} \Delta p \\ \Delta q \end{bmatrix},$$

(10)

in which $\Delta\varepsilon_{v+vw}$ is the total volumetric strain and $\Delta\varepsilon_{v+sw}$ is the total shear strain; d_{11}, d_{12}, d_{21}, and

d_{22} are defined as follows:

$$d_{11} = \frac{1}{B_e} + 2pA_1 - A_2\frac{q^s}{p^2} + \frac{a}{3\left(a + b\sigma_3\right)^2} ; \tag{11-1}$$

$$d_{12} = 0 ; \tag{11-2}$$

$$d_{21} = \frac{1}{B_e} - \frac{\sin\varphi\left(1 - \sin\varphi\right)q}{2\left(c\cos\varphi + \sigma_3\sin\varphi\right)^2} ; \tag{11-3}$$

$$d_{22} = 2A_1q + A_2\frac{sq^{s-1}}{p} + \frac{1 - \sin\varphi}{2c\cos\varphi + 2\sigma_3\sin\varphi} . \tag{11-4}$$

It is obvious that the stress-strain matrix in Equation (10) is not symmetric to the features of the double-yielding surface model.

NUMERICAL ANALYSIS OF WETTING-INDUCED DEFORMATION IN A ROCKFILL DAM

Model parameters

In the following sections, the constitutive model for the wetting-induced deformation that was previously proposed is used to analyze the wetting-induced deformation in a rockfill dam. The height of the dam is 139 m, the crest length is 42 m, and the crest width is 10 m. The material zoning and geometrical shape including the cross and longitudinal sections of the rockfill dam are shown in Fig. 3(a) and 3(b).
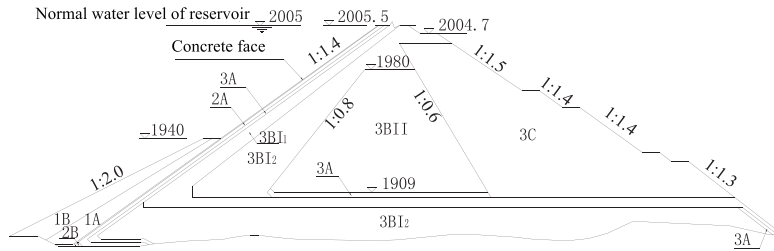
(a) Cross section and material zoning
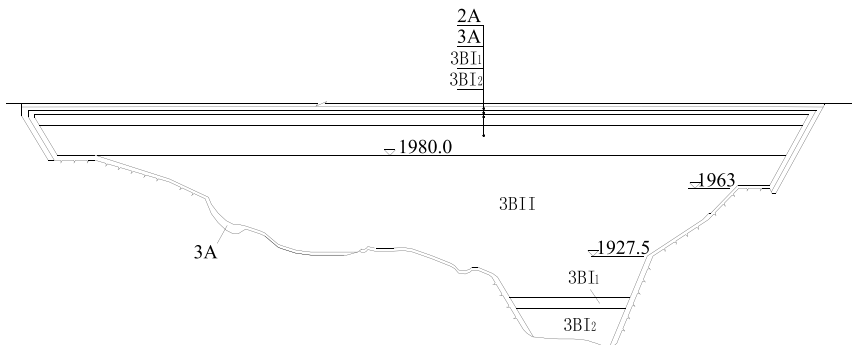
(b) Longitudinal section and material zoning

Figure 3. The material zoning and geometrical shape of the dam.

The main components of materials used in the dam are as follows: (i) the cushion materials (Zone 2A) are composed of slightly weathered granite and gneiss having a maximal particle size of 100 mm, and the quantity of particles smaller than 5 mm is 35%~45%. The designed dry density is 2.23 g/cm³; (ii) the transition zone materials (Zone 3A) are slightly weathered granite with a maximal particle size of 300 mm, and the quantity of particles smaller than 5 mm is 3%~17%. The designed dry density is 2.17 g/cm³; (iii) the main rockfill materials (Zones 3BI-1 and 3BI-2) are one of the main bearing parts of the dam and are also designed to be the drainage zone. The materials are slightly weathered granite and gneiss, in which the content of gneiss is lesser than 30%. The maximal particle size of these materials is 800 mm and the quantity of particles smaller than 5 mm is 8%. The designed dry density is 2.15 g/cm³; (iv) the main rockfill material (Zone 3BII) is sandy gravel with a maximal particle size of 450 mm, and the quantity of particles of size smaller than 5 mm is 15%~40%. The designed relative density is 0.8; (v) the secondary rockfill materials (Zone 3C) are fully gneiss, which are slightly weathered with a continuous grade distribution. The maximal particle size is 1000 mm, and the quantity of particles with size smaller than 5 mm is less than 35%. The parameters determined for the double-yielding surface model based on the test results of rockfill materials are shown in Table 1.

Table 1. Parameters of the double-yielding surface model.

Rockfill materials	ρ (g/cm³)	$\phi_0(°)$	$\Delta\phi(°)$	R_f	K	n	C_d	d	R_d
2A	2.15	49.4	8.7	0.826	1450	0.36	0.00083	1.320	0.82
3A	2.13	50.4	9.3	0.891	1390	0.34	0.00185	1.090	0.88
3BI-1	2.06	54.0	13.4	0.906	1422	0.26	0.00149	1.290	0.84
3BI-2	2.12	49.9	8.2	0.893	760	0.65	0.00948	0.387	0.80
3BII	2.14	47.4	6.0	0.842	690	0.31	0.00770	0.600	0.76
3C	2.11	49.5	9.4	0.810	550	0.47	0.00779	0.638	0.78

Note: $\varphi = \varphi_o - \Delta\varphi \lg\left(\sigma_3 / p_a\right)$.

Based on the triaxial wetting tests of the material in Zone 3BI-1 and compression wetting deformation tests of the materials in Zones 2A, 3A, 33BI-2, 3BII, and 3C, we can obtain the parameters in Equations (7) and (8) by fitting of the test results. To determine the sensitivities of these parameters of the rockfill materials to wetting-induced deformation, we selected two cases for fitting the test results. The first case involves fitting the test curve with a lower value (called Case 1) and the other case involves fitting the test curve with a middle value (Case 2) as shown in Fig. 4, which presents the selection of wetting volumetric strain parameters of the material in Zone 3BI-2. Furthermore, Case 3 and Case 4 are also defined by varying the parameters based on Case 1, which are shown in Table 2 (model parameters for wetting-induced deformation).
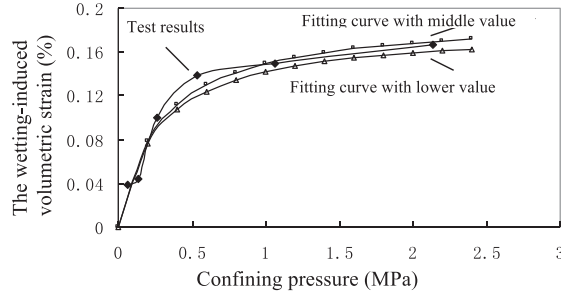
Figure 4. Selection of parameters of wetting volumetric strain of the material in Zone 3BI-2.

Table 2. Model parameters for wetting-induced deformation.

Rockfill material zone	Case 1			Case 2			Case 3			Case 4		
	b	a	D_w	b	a	D_w	b	a	D_w	B	a	D_w
2A	14.6	1.9	0.3*	17.0	1.9	0.3	17.0	1.9	0.6	17.0	1.9	0.9
3A	2.4	0.8	1.7*	2.6	0.8	1.7	2.6	0.8	3.4	2.6	0.8	5.1
3BI-1	1.0	1.2	0.9*	1.5	1.2	0.9	1.5	1.2	1.7	1.5	1.2	2.6
3BI-2	5.2	1.5	0.9	5.5	1.5	0.9	5.5	1.5	0.9	5.5	1.5	0.9

Note * indicates that the parameters were obtained by engineering analogy.

Phreatic line

Fig. 5 presents the phreatic lines for the cross section of 0+243. The variation in phreatic lines along the axis of the dam and its three-dimensional effects are considered in the numerical simulation of the wetting-induced deformation. Under steady seepage conditions, the tail water level is 1916 m. When considering the rise in tail water level, the phreatic lines are determined by the intersections of the horizontal lines at the elevations of 1920 m, 1930 m, and 1940 m and the original phreatic line. The phreatic lines under different tail water levels are shown in Fig. 5.
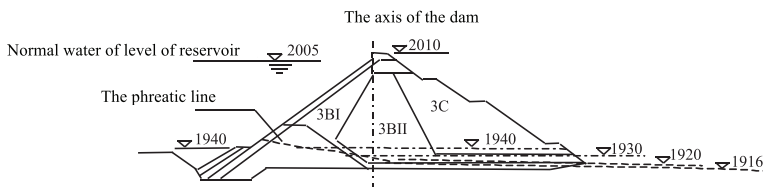
Figure 5. The phreatic lines for the cross section of 0+243.

Computational mesh

Fig. 6 presents the computational mesh partitioned according to the material zones of the dam body. The mesh has 7314 elements and 8555 nodes. The designed construction sequences are as follows: (i) the dam body is filled with a succession of horizontal layers and after the dam body was constructed, the concrete face enveloping it was constructed continuously; (ii) after the construction, water was filled up to the normal water level in the reservoir. The wetting-induced deformation is computed after the water was filled up to the normal water level in the reservoir.
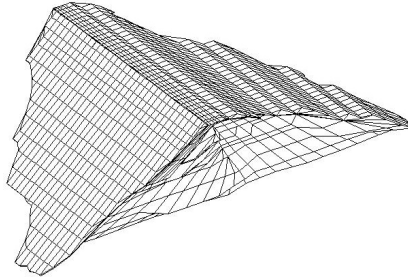
Figure 6. The computational mesh.

Computational results and analysis

(i) Effects of the elevation of tail water level: the computational results for the different cases under the conditions of steady seepage and rise in tail water level are presented in Table 3, from which we can find that there is an increase in the settlement of the dam body and an increase in the downstream horizontal displacement. These lead to increased extensive and compressive stresses in the horizontal direction of the face slab. Because of the compressive stress obtained through the incremental computational step, the peak value and zone corresponding to extensive stress in the face slab are reduced.

Table 3. Summary of the computed results.

Computed cases		Elevation of tail water level（m）	Horizontal displacement（cm）		Settlement（cm）	Deflection of face slab（cm）	Horizontal stress of face slab (MPa)		Stress of face slab along the slope (MPa)	
			Down stream	Upstream			Compression	Extension	Compression	Extension
Before wetting-induced deformation		------	13.6	8.7	55.4	14.8	5.3	2.6	2.4	3.5
Case 1：steady seepage		1916	14.8	8.0	60.6	19.9	9.3	4.2	6.5	0.7
Sensitivity analysis	Case 2	1916	14.8	8.0	60.2	19.5	9.0	4.0	5.8	0.8
	Case 3	1916	16.5	8.1	62.5	21.0	10.3	4.1	6.4	3.6
	Case 4	1916	18.4	8.2	65.2	22.5	11.6	4.6	7.8	3.7
Sensitivity analysis of downstream level		1920	17.3	8.0	61.8	19.9	9.3	4.3	6.3	0.8
		1930	19.9	8.1	63.5	21.0	9.5	4.3	7.3	0.7
		1940	21.9	8.3	65.2	22.3	9.5	4.1	7.5	0.6

Because of the wetting-induced deformation of rockfill materials under the phreatic line and the consequent lubrication between soil particles and weakening of minerals in the rockfill materials, the settlement of the dam body increases, and the horizontal displacement moves downstream. For example, under the steady seepage conditions of case 1, the maximal value of horizontal displacement moving downstream increases from 13.6 cm to 14.8 cm, the maximal value of horizontal displacement moving upstream decreases from 8.7 cm to 8.0 cm, and the maximal value of settlement increases from 55.4 cm to 60.6 cm. Fig. 7 presents the increment in the displacement of the dam body caused by wetting-induced deformation for the cross section of 0+243 under steady seepage conditions in case 1.
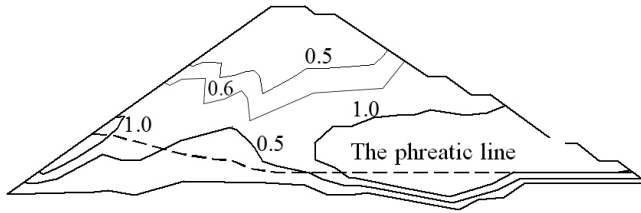
(a) The increase in horizontal displacement
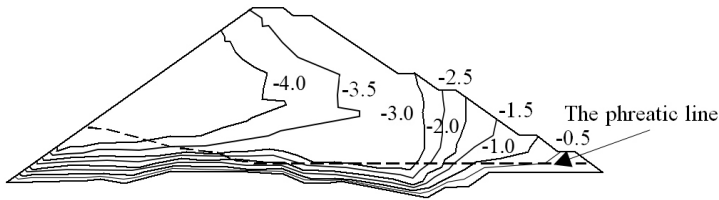
(b) The incremental increase in settlement

Figure 7. The incremental displacement of dam body caused by wetting under steady seepage conditions at the cross section of 0+243 under steady conditions in case 1 (unit: cm).

Because of the deformation induced by wetting, the dam body settles as a whole and displaces downstream, thus causing an increasing deflection of the face slab. For example, under the steady seepage conditions of case 1, the maximal value of deflection of the face slab increases from 14.8 cm to 19.9 cm; when the tail water level rises to 1940 m, the maximal value of deflection of the face slab increases from 14.8 cm to 22.3 cm as shown in Table 3. Fig. 8 gives the increase in face slab deflection due to the wetting-induced deformation.
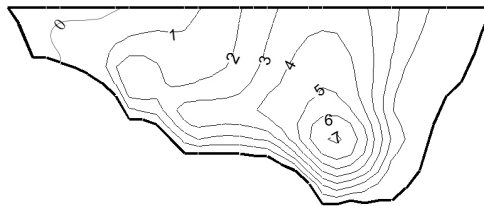
(a) Steady seepage with tail water level of 1916 m
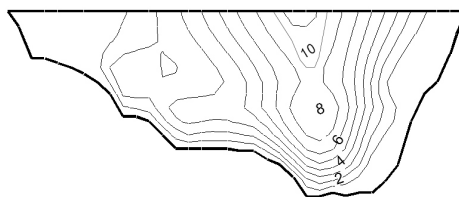
(b) Steady seepage with tail water level of 1940 m

Figure 8. Increment in face slab deflection due to the wetting-induced deformation (unit: cm).

In addition, due to the wetting-induced deformation, a relatively higher increment of compressive stress appears in the face slab, the peak value of compressive stress increases, the peak value of extensive stress along the slope surface decreases, and the peak values of both compressive and extensive stresses in the horizontal direction increase. For example, under the steady seepage conditions of case 1, the peak value of compressive stress of the face slab increases from 5.3 MPa to 9.3 MPa and that of the extensive stress of the face slab increases from 2.6 MPa to 4.2 MPa in the horizontal direction. Along the slope direction, the peak value of the compressive stress of the face slab increases from 2.4 MPa to 6.5 MPa and that of the extensive stress of the face slab increases from 3.5 MPa to 0.7 MPa as shown in Fig. 9.
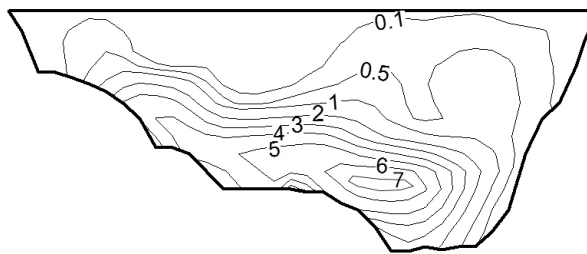
(a) The stress increment along the slope surface
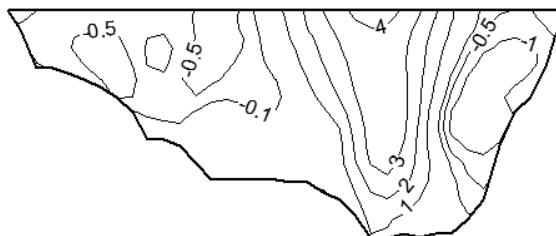
(b) The stress increment in the horizontal direction

Figure 9. Stress increment of the face slab due to the wetting-induced deformation under the conditions of the steady seepage (unit: MPa).

In the computed results of the wetting-induced deformation in Table 3, the maximal value of deflection of the face slab ranges from 19.9 cm to 23.3 cm, the peak value of stress of the face slab ranges from 5.8 MPa to 7.8 MPa, the peak value of extensive stress is 0.6 MPa~3.7 MPa along the slope surface, the peak value of compressive stress is 9.0 MPa~11.6 MPa, and the peak value of extensive stress is 4.0 MPa~4.6 MPa in the horizontal direction. When compared to the stress and displacement of the dam body when the reservoir has been filled with water, the increment in the maximal value of deflection of the face slab is 5.1 cm to 8.5 cm, the increment of the peak value of compressive stress of the face slab along the slope surface is 3.4 MPa~5.4 MPa, the reduction in the peak value of extensive stress of the face slab along the slope surface is 0.0 MPa~3.0 MPa, the increment in the peak value of compressive stress is 3.7 MPa~6.3MPa, and the reduction in the peak value of extensive stress is 1.4 MPa~2.0 MPa in the horizontal direction.

(ii) Study of parameters: in order to analyze the effects of the parameters of the wetting-induced

volumetric strain and axial strain on the deformation induced by wetting of dam body and behavior of face slab, the sensitivity of wetting parameters has been determined here. From the results in Table 3, it can be seen that reducing the parameters of wetting-induced volumetric strain rarely affects the horizontal displacement, and the maximal values of displacement in the horizontal direction corresponding to downstream and upstream are 14.8 cm and 8.0 cm, respectively. The vertical displacement decreases slightly with the increase in the maximal value from 60.6 cm to 60.2 cm, and the deflection of the face slab reduces from 19.9 cm to 19.5 cm. The peak value of the compressive stress of the face slab decreases from 9.3 MPa to 9.0 MPa and the peak value of the extensive stress of the face slab decreases from 4.2 MPa to 4.0 MPa in the horizontal direction. The peak value of the compressive stress of the face slab decreases from 6.5 MPa to 5.8 MPa, and the peak value of the extensive stress of the face slab decreases from 0.7 MPa to 0.8 MPa along the slope surface. With the rise in the tail water level, the horizontal displacement and vertical displacement of the dam body and deflection of the face slab increase according to similar distribution rules. For example, when the tail water levels are 1920 m, 1930 m, and 1940 m, the deflections of the face slab are 19.9 cm, 21.0 cm, and 22.3 cm, respectively. The tail water level also affects the stress distribution in the wall slab. The compressive stress of the face slab changes from 6.3 MPa to 7.5 MPa when the tail water level rises from 1920 m to 1940 m. However, its extensive stress changes from 0.8 MPa to 0.6 MPa along the slope surface.

DISCUSSIONS

The following discussions pertain to the constitutive model used in this study. The double-yielding surface model was first proposed by Shen in 1981 and revised later in 2000 (Shen, 2000). Compared to the Cam-Clay model, it can model the dilatancy of coarse-grained soil at a lower confining pressure by introducing a shear-yielding surface along with usage of the volumetric-yielding surface employed in the Cam-Clay model. Most rockfill materials exhibit strain-hardening at all confining pressures, volumetric contraction followed by dilatancy at lower confining pressures, and volumetric contraction at higher confining pressures. The rockfill materials in the rockfill dam, which were numerically analyzed in the paper, show stress-strain and volumetric deformations, which can be modeled using the double-yielding surface model. Therefore, the double-yielding surface model proposed by Shen (2000) was used as a basic model-to-model study of wetting-induced deformation of rockfill materials.

The wetting-induced volumetric strain expressed in Equation (7) indicates that the confining pressure affects the volumetric strain caused by wetting. However, the wetting-induced shear strain expressed in Equation (8) indicates that the deviatoric stress and strength parameters affect the shear strain caused by wetting because of the stress level. When formulating the expression for the wetting-induced deformation, we consider its simpler form for performing numerical computation. Therefore, Equations (7) and (8) are employed, in which all the influential factors such as confining pressure, deviatoric stress, strength parameters, and model constants are considered. There are several complex factors that influence the wetting-induced deformation, which can be investigated in the future.

The constitutive model is dependent on the density of the rockfill dam, but the initial stress

caused by its weight can be different at different locations of the rockfill materials in the dam. This may be reflected in the initial stress of the dam. The constitutive model proposed here does not consider the influence of the density of rockfill materials, which can be a part of a further study on this topic.

The height of the dam was 139 m. Therefore, the stress level was low, and particle crushing could be neglected. If the height of the dam reaches 300 m, the particles may break up and cause heavy volumetric contraction. The constitutive model proposed here should be extended to consider the influence of particle breakage when studying the wetting-induced deformation of a high dam with height in the range of 200 m–300 m.

CONCLUSIONS

A computational method for determining the wetting-induced deformation of rockfill dams is proposed here. This method was employed to perform wetting-deformation analysis of a concrete-faced rockfill dam under the conditions of steady seepage and rise in tail water table. Some conclusions can be summarized as follows:

(i) The revised constitutive model for computing the wetting-induced deformation can be used to predict the wetting-induced deformation of rockfill dams by considering the effect of confining pressure on the wetting-induced volumetric strain.

(ii) When wetting-induced deformations of rockfill materials occur under the phreatic line, the settlement of dam body increases, and the horizontal displacement moves downstream. The dam body settles as a whole and undergoes displacement in the downstream direction. This causes an increase in the deflection of the face slab. A relatively higher increment of the compressive stress appears in the face slab leading to an increase in the peak value of the compressive stress and a reduction in the peak value of the extensive stress along the slope surface, and the peak values of the compressive and extensive stresses increase in the horizontal direction.

ACKNOWLEDGMENT

REFERENCES

Alonso, E. E., Gens, A. & Josa, A. 1990. A constitutive model for partially saturated soils. Geotechnique **40**(3): 405-430

Cen, W., Erich, B. & Sendy, F.T. 2009. Application of Gudehus-Bauer hypoplastic model of core-wall type rockfil ldams considering wetting behavior. Rock and Soil Mechanics, **30**(12):3808-3812. (In Chniese)

Duncan, J.M. & Chang, C.Y. 1970. Nonlinear analysis if stress and strain in soils. Journal of Geotechncial Engineering, ASCE, **96**: 1629-1652.

Escuder, I., Andreu, J. & Rechea, M. 2005. An analysis of stress strain behaviour and wetting effects on quarried rock shells.Canadian Geotechnical Journal, **42**(1): 51-60

Ferber, V., Auriol, J. C., Cui, Y. J. & Magnan, J. P. 2008. Wetting induced volume changes in compacted silty clays and high plasticity clays. Can. Geotech. J., **45**(2): 252-265

Nobari, E. S. & Duncan, J. M. 1972. Effect of reservoir filling on stresses and movement in earth and rockfill dams: a report of an investigation [R].Vicksburg: Waterways Experiment Station.

Roosta, R.M. & Alizadeh, A. 2012. Simulation of collapse settlement in rockfill material due to saturation. International Journal of Civil Engineering, **10**(2): 93-99.

Saboya, F. & Byrne, P.M. 1993. Parameters for stress and deformation analysis of rockfill dams. Canadian Geotechnical Journal, **30**(3): 690-701.

Shen, Z.J. 2000. Theoretical Soil Mechanics. China Water Power Press, Pp. 53-54.

Zou, D., Yang, X, Liu, J, Kong, X. & Zhou Y. 2015. Numerical analysis of wetting-induced deformation of Xiyu conglomerate gravel dam with asphalt concrete core. Journal of Dalian University of Technology, **55**(6):605-611.

Zhu, B.L. & Shen, Z.J. 1990. Computational soil mechanics. Shanghai Science and Technology Press, Shanghai.